

SiCP: Simultaneous Individual and Cooperative Perception for 3D Object Detection in Connected and Automated Vehicles

Deyuan Qu¹ Qi Chen² Tianyu Bai¹ Andy Qin¹ Hongsheng Lu²
 Heng Fan¹ Song Fu¹ Qing Yang¹
¹University of North Texas, ²Toyota InfoTech Labs

Abstract

Cooperative perception for connected and automated vehicles is traditionally achieved through the fusion of feature maps from two or more vehicles. However, the absence of feature maps shared from other vehicles can lead to a significant decline in object detection performance for cooperative perception models compared to standalone 3D detection models. This drawback impedes the adoption of cooperative perception as vehicle resources are often insufficient to concurrently employ two perception models. To tackle this issue, we present *Simultaneous Individual and Cooperative Perception (SiCP)*, a generic framework that supports a wide range of the state-of-the-art standalone perception backbones and enhances them with a novel *Dual-Perception Network (DP-Net)* designed to facilitate both individual and cooperative perception. In addition to its lightweight nature with only 0.13M parameters, DP-Net is robust and retains crucial gradient information during feature map fusion. As demonstrated in a comprehensive evaluation on the OPV2V dataset, thanks to DP-Net, SiCP surpasses state-of-the-art cooperative perception solutions while preserving the performance of standalone perception solutions. The code link is <https://github.com/DarrenQu/SiCP>.

1. Introduction

Cooperative perception leverages wireless connectivity among vehicles to exchange sensor information, fostering a collective understanding of the driving environment. In contrast to individual perception, where a vehicle relies solely on local sensor data, cooperative perception creates a local map that extends beyond line-of-sight, enhancing vehicle navigation over an extended space and time horizon.

Within the realm of cooperative perception, feature map sharing-based approaches exhibit significant promise due to their superior performance and modest demands on the wireless channel capacity. Notable works in this domain, such as F-Cooper [2], AttFuse [26], Where2Comm [10] and

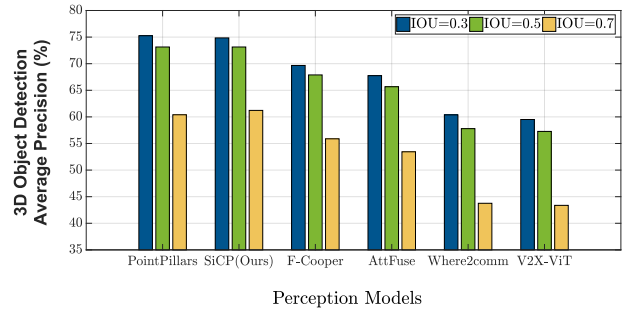


Figure 1. Comparison of LiDAR-based 3D object detection performance among different perception models. Except PointPillars [13], all others are cooperative perception models operating without over-the-air feature maps. The performance of individual perception mode is important as features shared by other vehicles may not be always available. Our SiCP model shows no performance degradation as compared to PointPillars [13].

V2X-ViT [25], have showcased the superiority of cooperative perception over its individual counterparts.

However, a critical issue overlooked by these prior works poses a challenge to the potential widespread adoption of their solutions. Specifically, they assume vehicles either exclusively use a cooperative perception model for both individual (in absence of feature maps from peers) and cooperative perception tasks or possess sufficient resources to concurrently employ two models, each dedicated to a different perception mode. Both assumptions present challenges, e.g., the former leads to performance degradation when the cooperative perception model operates in individual perception mode, as illustrated in Figure 1. Several cooperative perception models consistently lag behind PointPillars [13], the sole individual perception model, across all evaluated Intersection-Over-Union (IOU) thresholds in individual perception mode, with a detection precision gap reaching as high as 17.03%. Meanwhile, the latter assumption encounters practical hurdles, as vehicles often have limited hardware and software resources to support more than one perception solution. Existing cooperative perception models typically demand a larger memory footprint and

computing power than individual perception solutions, posing obstacles to deployment. Hence, the community needs a cooperative solution that is lightweight and exhibits no performance degradation when operating in individual perception mode.

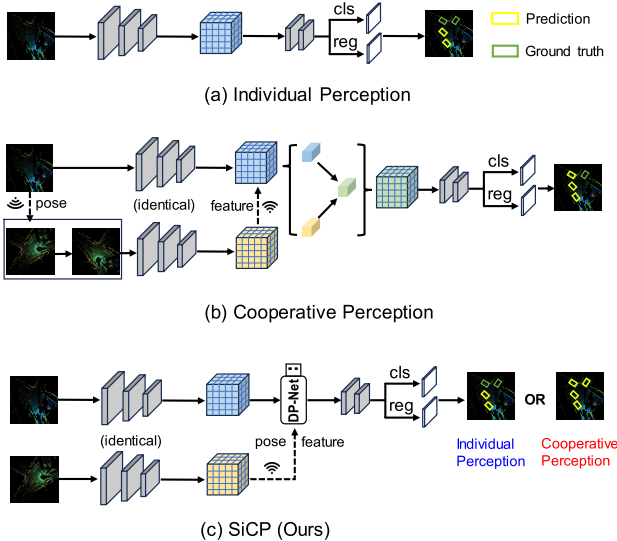


Figure 2. Different approaches to perception. In (a), individual perception uses local sensor data for object detection. Cooperative perception, shown in (b), combines data from various vehicles to enhance the ego-vehicle’s perception. Simultaneous Individual and Cooperative Perception (SiCP), as depicted in (c), supports both functionalities simultaneously.

1.1. Proposed Solution

We introduce an innovative perception framework, SiCP (Simultaneous Individual and Cooperative Perception), offering a versatile and unified solution to concurrently support individual and cooperative perceptions. Illustrated in Figure 2 (c), SiCP comprises three key components: a feature extractor, a feature processor, and a detection head. This architecture is intentionally designed to align with popular pipelines of both individual perception models (Figure 2 (a)) and cooperative perception models (Figure 2 (b)). This alignment facilitates the seamless transformation of singular-function perception solutions into dual-mode perception systems.

More specifically, the feature extractor of SiCP generates features catering to both perception modes, storing them locally and transmitting them for cooperative perception at neighboring vehicles. To maintain manageable communication demands, we generate features based on the sender vehicle’s perspective, eliminating the need for the sender vehicle to compute and share features individually with each nearby receiver as in [15]. An initial affine transformation in the feature processor aligns the received features’ perspective with the receiver vehicle’s.

SiCP’s feature processor orchestrates local and received features to optimize object information representation. Housing a novel Dual-Perception network (DP-Net), it acts as a conduit for local features in individual perception mode while efficiently performing feature fusion in the presence of received features. This fusion component effectively preserves and combines gradient information from both local and received features, enabling the detection of objects not recognizable using local or received features alone in cooperative perception mode. Further details about the feature processor are provided in Section 3.1.

In SiCP’s detection head, we adopt a standard architecture as seen in [13]. However, we tailor its loss function to accommodate losses from both individual and cooperative perceptions. Special attention is given to the training strategy to balance the loss ratio from each perception mode, facilitating the feature extractor in capturing patterns useful for both modes. Our performance evaluation shows that SiCP excels in both individual and cooperative perception.

It’s important to note that unlike other cooperative perception models [25, 26], SiCP fuses feature maps from only two vehicles in a single forward propagation. This design choice is motivated by the reality that a vehicle has to wait longer to accumulate feature maps from more neighbors. Given the lossy nature of wireless communication, it is uncertain if a feature map from a third surrounding vehicle will ever arrive. To counteract delays that offset the benefits of cooperative perception, SiCP focuses on fusing feature maps from one vehicle at a time. Different neighboring vehicles’ feature maps can be selected at different times, especially when multiple connected and automated vehicles are available.

1.2. Main Contributions

The contributions of this work are as follows:

- For the first time, we recognize the significance of simultaneous individual and cooperative perception in connected and automated vehicles.
- The proposed solution excels in cooperative perception task, surpassing the state-of-the-art models in performance, while achieving result on par with leading standalone 3D detection models in individual perception task.
- The proposed DP-Net is a Plug-and-Play module as it can be seamlessly integrated into other individual perception models, enabling simultaneous individual and cooperative perception.
- The proposed DP-Net is also a lightweight component, comprising just 0.13M parameters, representing a mere 1.7% increase from the PointPillars [13] backbone model.
- The proposed SiCP framework will facilitate the exploration of novel and effective designs for feature extractors, feature fusion, and detection heads, enabling simultaneous individual and cooperative perception.

2. Related Works

2.1. Individual Perception

LiDAR-based 3D object detection plays a crucial role in the perception system of automated vehicles, effectively aiding in determining the size, position, and category of nearby 3D objects. Currently, standalone 3D object detection models fall into two main categories: point-based and voxel-based. Point-based models, such as those proposed in [17, 18, 20], directly process unstructured point clouds, extracting features directly from the raw data. On the other hand, voxel-based methods, as exemplified by [13, 27, 31], transform point clouds into structured voxel or pillar formations. These methods adeptly balance computational performance with capturing essential spatial details. Despite their strengths, both point-based and voxel-based methods face limitations in perception range and accuracy due to sensor constraints and the complexity of real-world road conditions. To address these challenges, there is a growing trend towards cooperative perception, which involves combining data from multiple vehicles, enhancing detection capabilities and overcoming individual perception limitations.

2.2. Cooperative Perception

Cooperative perception solutions for connected and automated vehicles can be classified into *early fusion* [1, 3], *deep fusion* [2, 4, 9, 14, 15, 19, 21, 22, 25, 26, 29], and *late fusion* [5, 6, 8, 30]. Among these, the deep fusion method strikes a balance between bandwidth and detection performance, making it widely embraced in the literature.

Activation function based fusion. Initially introduced in [2], F-Cooper employs the *maxout* operation for feature map fusion. CoFF [9] enhances F-Cooper by incorporating feature enhancement techniques. Despite their advancements, these solutions grapple with challenges stemming from the heterogeneity of feature maps originating from different vehicles. Even when focusing on the same region, perceptual differences can result in significantly varied features.

Attention based fusion. AttFuse [26] incorporates a self-attention operation for feature fusion. Despite its effectiveness, the solution overlooks nearby features, missing out on crucial information locality. V2X-ViT [25] introduces a unified transformer architecture for heterogeneous multi-agent perception, while COOPERNAUT [4] adopts a transformer-based architecture with point-based representations. While these solutions consider self-attention relations among all points in feature maps, making them computationally intensive, they are less focused on specific regions.

Other models adopt diverse strategies for feature fusion from various perspectives. For instance, Where2comm [10] introduces a spatial confidence map to capture the spatial diversity of perceptual data, effectively minimizing com-

munication bandwidth. V2VNet [22] employs a variational image compression algorithm to compress features and utilizes the mean operation for feature aggregation. DiscoNet [14] employs a teacher-student distillation method that combines early and deep fusion techniques. Additionally, CoAlign [15] introduces a novel hybrid collaboration framework designed to address pose errors. Furthermore, Camera-LiDAR frameworks enhance cooperative perception with camera support [23].

While these methods demonstrate excellence in cooperative perception, they often overlook the models’ processing capabilities for individual tasks. In contrast, our proposed approach not only excels in cooperative perception but also ensures outstanding performance in individual perception.

3. Methodology

This section outlines the major components of the SiCP (Simultaneous Individual and Cooperative Perception) framework, illustrated in Figure 3. The framework comprises three key elements: a *feature extractor*, an *Dual-Perception Network*, and a *unified detection head*. We adopt the backbone of PointPillars [13] as our *feature extractor*, aiming to achieve an optimal balance between effectiveness and efficiency in 3D object detection. We propose the Dual-Perception Network (DP-Net) that seamlessly integrates with the existing backbone (Section 3.1), adeptly processing local features for individual perception and fusing features from multiple vehicles for cooperative perception. We employ a unified detection head (Section 3.2) to process features in both individual and cooperative perception tasks. The proposed solution operates on the premise of vehicular trustworthiness, with all vehicles employing the same machine-learning model for executing their object detection tasks.

3.1. Dual-Perception Network (DP-Net)

The proposed DP-Net module should ensure that the individual perception process and cooperative perception process run in parallel. Moreover, the resulting feature maps, whether for individual or cooperative perception, should be compatible with each other and capable of being processed by a unified detection head. Specifically, DP-Net executes operations based on whether the ego vehicle has received features from neighboring vehicles. In the absence of received features, DP-Net continues utilizing the current ego vehicle’s feature maps, thereby guaranteeing its individual perception performance. Upon receiving features from neighboring vehicles, DP-Net performs a perspective transformation on these features before forwarding them to the fusion module for integration. We will delve into the critical endeavor of effectively fusing feature maps in Sections 3.1.1 and 3.1.2.

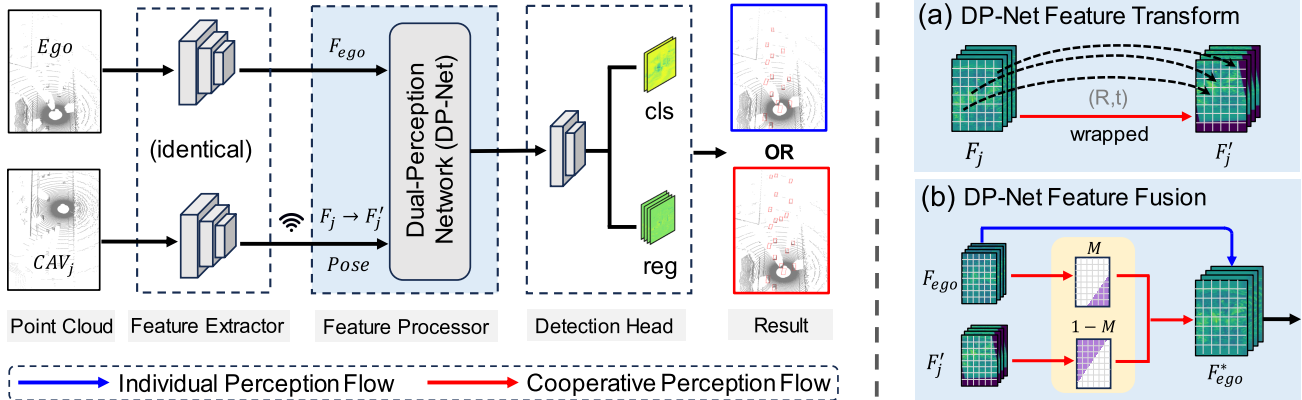


Figure 3. An overview of the SiCP architecture showcases its components: a feature extractor, a feature processor (DP-Net), and a detection head. All vehicles have identical feature extractors producing fusible features. The feature processor manages local features F_{ego} for individual perception and fused features F_{ego}^* for cooperative perception. Features from other vehicles (e.g., F_j) are transformed to the ego vehicle’s perspective (as shown in (a)) and integrated with local features using the DP-Net module (as shown in (b)). The resulting feature F_{ego}^* is then processed by the detection head to generate classification and regression results for either individual or cooperative perceptions.

3.1.1 Receiver-Agnostic Feature Sharing

To enable cooperative perception through deep fusion, vehicles must share their locally generated features with nearby vehicles. Achieving efficient vehicular communications requires implementing a receiver-agnostic feature-sharing approach, wherein the sender does not need to know the location and pose of the potential receivers. However, implementation of existing methods often require transforming LiDAR data or feature maps into the perspective of the receiving vehicle before transmission [19, 21, 25, 26, 29]. In scenarios involving multiple receiving vehicles, this results in creating and transmitting multiple versions of the same feature maps, leading to significant network traffic and computational demands on the sending vehicle. Alternatively, the sending vehicle can optimize its communication by broadcasting its local feature map to all nearby vehicles. In this approach, the sending vehicle shares not just its feature map but also its current location and pose information. Upon receiving a shared feature map, the recipient vehicle performs feature transformation using the Affine Transformation technique [15].

3.1.2 Complementary Feature Fusion

An essential element of the DP-Net is a fusion module that efficiently merges the received feature map with the locally generated one on the ego vehicle. This fusion mechanism depends on preserving gradients within the feature maps earmarked for integration.

Gradients Matter in Fusion. Our study has uncovered a useful insight into the features associated with vehicle objects. As depicted in Figure 4, features located near the edges of a vehicle exhibit distinct characteristics,

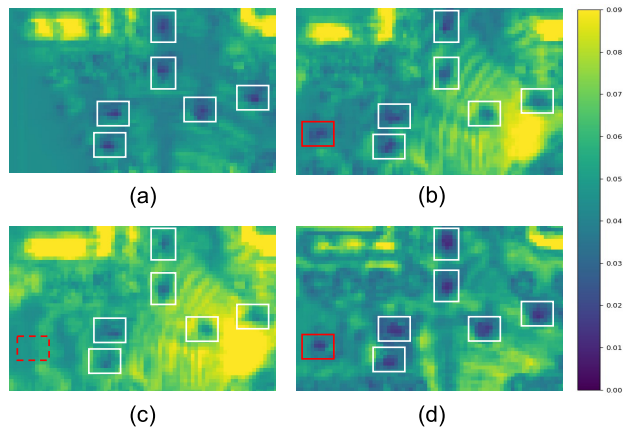


Figure 4. Gradient information is lost during the fusion of feature maps. In (a), a receiver’s feature map clearly indicates six objects but misinterprets one object (red rectangle, as shown in (b)) in the sender’s feature map. Upon fusion of these maps using the *maxout* function, the gradients of this particular object (red dotted rectangle) vanish, as shown in (c). Our method can effectively preserve the gradient during the feature fusion process, as shown in (d).

however, the central regions of the object lack distinctive features. This occurrence can be attributed to the scarcity or absence of LiDAR-generated points within the internal empty spaces of a vehicle. In contrast, the vehicle’s body effectively reflects LiDAR signals, generating strong features.

Differences in the LiDAR point cloud data acquired by different vehicles can result in varying features for the same object/vehicle. Due to occlusions, the receiver has difficulty in capturing meaningful features for one object, indicated by the red box in Figure 4 (b). Consequently, the resulting feature maps might misinterpret these regions as back-

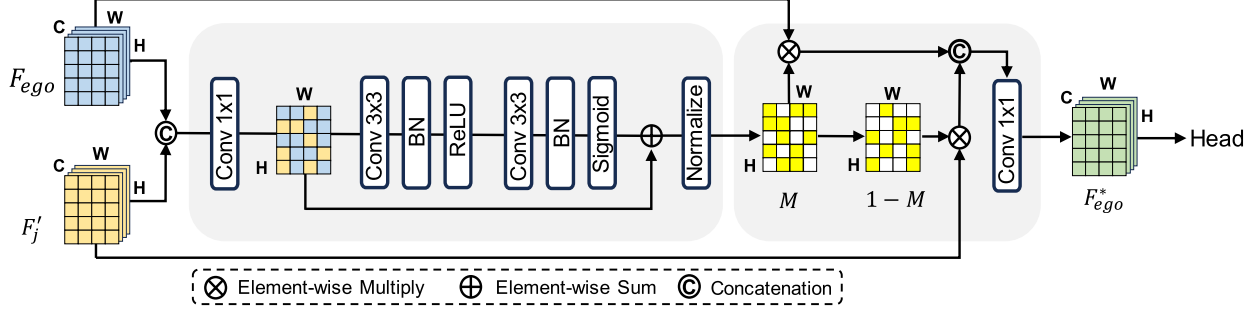


Figure 5. Complementary Feature Fusion efficiently merges two BEV (Bird’s Eye View) feature maps by learning a weighted map. Initially, it concatenates the two feature maps and condenses them into a one-channel feature map, using a 1x1 convolutional operation. This resultant feature map undergoes processing through two convolutional layers, generating the weighted map M . M adjusts the ego vehicle’s local feature map, whereas the complementary weighted map $(1 - M)$ modifies the received feature map. Finally, the two feature maps are concatenated and reshaped to the size of $H \times W \times C$.

ground, resulting in relatively larger numerical representations. When the feature maps from the sender and receiver are fused using the basic *maxout* function, the gradients in the sender’s features vanish due to the influence of the larger numbers in the receiver’s feature map.

Gradients Perseverance in Fusion. Expanding on the insights derived from the above analysis, we present a novel fusion module. This fusion process is named as *complementary feature fusion*, as illustrated in Figure 5. The pipeline is designed not only to prioritize the retention of gradients during the fusion process but also to harness the complementary data contributed by other vehicles.

Let’s assume the ego vehicle receives a feature map \mathcal{F}_j from another automated vehicle j , along with its pose \mathcal{P}_j and location \mathcal{L}_j information. Based on the Affine Transformation $\Psi(\cdot)$, we warp the sender’s feature map to the ego-vehicle’s perspective to get the transformed feature map $\mathcal{F}'_j = \Psi(\mathcal{F}_j)$. We concatenate the ego vehicle’s feature map \mathcal{F}_{ego} and the transformed \mathcal{F}'_j . The concatenated feature map is then processed by a 1×1 convolutional layer. This process can be summarized as

$$\Phi = Conv(\mathcal{F}_{ego} \parallel \mathcal{F}'_j) \in \mathbb{R}^{H \times W} \quad (1)$$

where Φ is the resulting feature map, \parallel denotes the concatenation operation. Here, we utilize a 1x1 convolutional operation to handle stacked feature maps and produce a unified single-channel feature map. This step can be substituted with similar operations such as maxout or averaging operations.

To make use of the aggregated feature map, we follow it with a second operation to fully capture spatial dependencies. Specifically, we employ a the following operation to get a weight map $\tilde{M} \in \mathbb{R}^{H \times W}$:

$$\tilde{M} = \Phi \oplus (\sigma(BN(Conv(\delta(BN(Conv(\Phi))))))) \quad (2)$$

where BN denotes the Batch Normalization [11], δ and σ refer to the ReLU and Sigmoid functions [16], and \oplus de-

notes element-wise summation. Here, we apply two layers of 3×3 convolutional operations.

Next, we normalize \tilde{M} to get a normalized weighted map M , in which all the numbers range within $[0, 1]$. As M is used to weigh and fuse features from two feature maps, we further adjust M as follows. For any element m_{ij} in M , we have

$$m_{ij} = \begin{cases} m_{ij}, & m_{ij} \in \mathcal{F}_{ego} \cap \mathcal{F}'_j \\ 0, & otherwise \end{cases} \quad (3)$$

As such, the weight map M only provides clues to fuse the features within the overlapping area between \mathcal{F}_{ego} and \mathcal{F}'_j . While for the non-overlapping area, the weight map is always 0. This implies the ego vehicle does not consider other vehicles’ data but only relies on its own to detect objects.

After fusing with the received feature map, the ego vehicle’s feature map will be updated to $\mathcal{F}_{ego}^* \in \mathbb{R}^{C \times H \times W}$ by the following operations:

$$\mathcal{F}_{ego}^* = Conv\left((M \otimes \mathcal{F}_{ego}) \parallel ((1 - M) \otimes \mathcal{F}'_j)\right) \quad (4)$$

where \otimes denotes the element-wise multiplication. Note that the weight map M is responsible for adjusting the ego vehicle’s location feature map, while the complementary weight (CW) map $(1 - M)$ modifies the received feature map. This means, in the fused feature map, each point is strongly influenced either by the ego vehicle’s feature or by the other vehicle’s feature, but not both simultaneously.

3.2. Detection Head

The DP-Net we propose generates two potential outcomes: the feature map of the ego vehicle and the fused feature map. To maintain compatibility with existing detection models, it is crucial to establish a unified detection head capable of efficiently handling both types of feature maps. In this context, we employ a single detection head to manage both individual and cooperative perception, ensuring that

the loss functions for each scenario share a consistent format. The loss function utilized in our model aligns with the one employed in the PointPillars model [13].

To realized effective training, we need to ensure an equitable distribution of training data for individual and cooperative perception tasks. Due to resource limitations, conducting additional training rounds is unfeasible. Both individual and cooperative perception components in the proposed model must be trained using a single input data and labels. Therefore, the total number of training rounds remains constant. Specifically, our methodology involves inputting a single data instance, encompassing the raw local LiDAR data and a feature map shared by another vehicle, into the network. Then, backpropagations are applied, allowing the individual perception and cooperative perception pipelines to be trained jointly.

4. Experiments

Datasets. We conduct our evaluations using the OPV2V dataset [26] which is a simulation dataset for V2V cooperative perception, co-simulated through OpenCDA [24] and CARLA [7]. In accordance with the particular training and testing specifications of our model, we implement a First-Come-First-Serve policy for each frame in the dataset. This approach facilitates the utilization of data from two vehicles: the ego vehicle and the sender vehicle. Following [26], the LiDAR detection range of each vehicle to be $x \in [-140.8m, 140.8m]$ and $y \in [-40m, 40m]$, and the communication range between vehicles is $70m$.

Training. Our SiCP model enhances learning efficiency through joint training of individual and cooperative perception. The gradients obtained from these two tasks are backpropagated sequentially to update the parameters of the backbone, DP-Net, and the detection head. Due to the equal amount of training data and identical backbone parameters, the entire network receives an equivalent amount of training, regarding individual and cooperative perceptions. This balanced training approach equips our model to effectively handle SiCP tasks, even when dealing with limited training data. It’s worth noting that our end-to-end training method eliminates the need for pre-training any parameters. We train the model with one Nvidia RTX 3090 GPU and employ the Adam optimizer [12] with a learning rate of 0.001 and a batch size of 1 in our model training process.

Inference. At the inference stage, we use the average precision (AP) metric to evaluate the performance of all models on two OPV2V test sets (Default and Culver). The evaluation involved employing IoU thresholds of 0.5 and 0.7, respectively.

Baselines. To facilitate comparison, we construct two baseline models dedicated to cooperative and individual perception. In the cooperative perception task, late fusion aggregates prediction outcomes from multiple agents, employ-

ing Non-Maximum Suppression (NMS) to produce the final results. Furthermore, we evaluate individual perception results against state-of-the-art standalone 3D detection networks such as PointPillars [13], PIXOR [28], SECOND [27], and VoxelNet [31]. Notably, SiCP diverges from established benchmarks where vehicles must initially project their individual point clouds onto the ego vehicle’s viewpoint; instead, our implementation mandates each vehicle to exclusively process data from its own perspective, mirroring real-world data-sharing scenarios among connected vehicles.

4.1. Quantitative Evaluations

In the comparative analysis, we assess our model against existing benchmarks from two distinct perspectives: *individual perception* and *cooperative perception*. Our findings reveal that SiCP outperforms all other cooperative solutions, meanwhile, SiCP demonstrates satisfactory performance for individual perception scenarios.

Cooperative Perception. Regarding cooperative perception, as shown in Table 1, SiCP achieves an impressive 85.72% AP with an IoU of 0.5, surpassing the second-best solution (AttFuse) which offers an 82.75% AP. Compared to the benchmark F-Cooper, SiCP exhibits a notable 8.2% enhancement. This improvement is attributed to the incorporation of the complementary feature fusion, which carefully merges two feature maps by learning optimized weights for every position within the overlapping feature map. The weights assigned to the ego vehicle and sender vehicle are mutually complementary, aligning seamlessly with the inherent logic of fusing feature maps.

Table 1. Comparison of cooperative perception performance

Methods	Default		Culver	
	AP@0.5	AP@0.7	AP@0.5	AP@0.7
Late Fusion	75.09	69.79	66.92	60.99
F-Cooper[2]	77.52	62.95	57.62	44.54
AttFuse[26]	82.75	72.63	72.02	59.76
V2X-ViT[25]	82.14	65.81	75.16	55.81
Where2comm[10]	78.72	64.84	75.84	59.04
SiCP (Ours)	85.72	73.64	77.49	62.42

Individual Perception. Traditional cooperative solutions like F-Cooper [2], AttFuse [25], Where2comm [10], and V2X-ViT [25], are designed to tackle cooperative perception challenges and do not consider individual perception at all. Therefore, when they are applied to process the data generated solely by the ego vehicle, their performance declines significantly. As shown in Table 2, the performance of V2X-ViT drops by 17.03%, compared to the standalone model PointPillars when the IoU is set at 0.7. This underscores the significance of considering individual perception in the design of cooperative perception models.

Our developed SiCP solution showcases a significant improvement, with its performance closely approaching that of the best standalone models. The strength of our model stems from its specialized dedicated pipeline for individual perception, utilizing features derived solely from the ego vehicle.

Table 2. Comparison of individual perception performance

Methods	Default		Culver	
	AP@0.5	AP@0.7	AP@0.5	AP@0.7
PointPillars [13]	73.14	60.40	69.57	57.11
PIXOR [28]	61.34	40.04	48.84	33.48
SECOND [27]	72.85	62.63	70.53	59.32
VolxNet [31]	66.41	52.23	66.80	50.72
F-Cooper [2]	67.89	55.88	63.73	52.36
AttFuse [26]	65.67	53.44	64.13	51.60
V2X-ViT [25]	57.27	43.37	64.81	47.16
Where2comm [10]	57.79	43.76	66.51	51.49
SiCP (Ours)	73.14	61.22	69.67	56.53

4.2. DP-Net is a Lightweight Plug-and-Play Module

We conduct a comparative analysis involving two pairs of comparisons, each comprising an original backbone model and the one extended by integrating DP-Net. The selected standalone 3D detection backbones are two representative network architectures in the field of 3D object detection: PointPillars [13] and VoxelNet [31]. As demonstrated in Table 3, DP-Net consistently demonstrates improvement across all baseline 3D detection backbones. These findings underscore the generic applicability of DP-Net, suggesting its potential to be integrated into other 3D object detection frameworks. Moreover, the proposed DP-Net is a lightweight solution as it does not significantly increase the number of parameters requiring training, i.e., DP-Net consists of only 0.13M parameters. If the underlying backbone is PointPillars, with a set of 7.27M parameters to be trained, the introduction of DP-Net increases the overall parameters by a mere 1.7%. With its lightweight design, SiCP achieves a latency of just 37.84ms.

Table 3. Existing 3D detection backbones can be extended by integrating DP-Net to address cooperative perception.

Backbones	Methods	Default		Culver	
		AP@0.5	AP@0.7	AP@0.5	AP@0.7
PointPillars [13]	IND	73.14	60.40	69.57	57.11
	+DP-Net	85.72	73.64	77.49	62.42
VoxelNet [31]	IND	66.41	52.23	66.80	50.72
	+DP-Net	83.44	72.67	78.71	70.91

4.3. Qualitative Evaluations

More qualitative results for individual perception are presented in Figure 6. Specifically, Figure 6 (a) showcases

detection errors for F-Cooper, (b) illustrates errors for AttFuse, (c) displays errors for V2X-ViT, and (d) demonstrates errors of SiCP. The figure highlights instances of false positive and false negative detection results, attributed to incorrect feature extraction in existing cooperative solutions while attempting to address the individual perception task. In contrast, the SiCP method incorporates both individual and cooperative perception during feature extraction, leading to more precise object detection results.

Regarding cooperative perception, as depicted in Figure 7, our proposed SiCP model also exhibits significantly fewer false negative and false positive detection results in comparison to (a) F-Cooper, (b) AttFuse, and (c) V2X-ViT. Notably, we observe a higher incidence of false negative detections in cooperative perception, compared to the individual perception scenarios. This is because any erroneous fusion can generate features that fail to indicate objects accurately, thereby causing false negatives. The superior performance of SiCP is attributed to DP-Net, which effectively fuses features and generates a more precise representation of objects within the feature maps.

4.4. Ablation Study

Impact of Complementary Fusion. To better understand the DP-Net, particularly the importance of complementary feature fusion, we exclude the branch responsible for applying the complementary weights (CW) to the received feature maps. As demonstrated in Table 4, the incorporation of the CW map results in a noteworthy enhancement in performance metrics, both at AP@0.5 and AP@0.7. This underscores the importance of weighting feature maps in a complementary fashion, emphasizing its pivotal role in augmenting the accuracy of object detection.

Table 4. Importance of complementary weights (CW)

Method	Default		Culver	
	AP@0.5	AP@0.7	AP@0.5	AP@0.7
w/o CW	84.76	70.16	78.32	61.70
w. CW	85.72	73.64	77.49	62.42

Impact of 1x1 Convolutional Layer. In the complementary feature fusion architecture, the stacked BEV feature maps need to be dimensionally reduced from 512 channels to 1 channel. We opt for a 1x1 convolutional layer for this purpose, facilitating feature interaction across channels. Although alternative methods exist, our experiments in Table 5 reveal that 1x1 convolutions mostly outperform other alternatives.

Impact of Number of Convolutional Layers. We incorporate two convolutional layers within the complementary feature fusion to learn the weight map. As shown in Table 6, increasing the convolutional layer number from 1

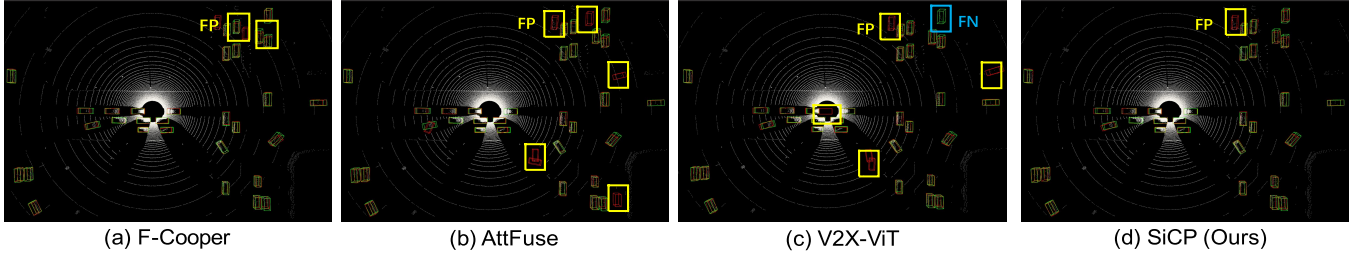


Figure 6. Illustrations of false positive (yellow) and false negative (blue) detection results for the individual perception scenarios.

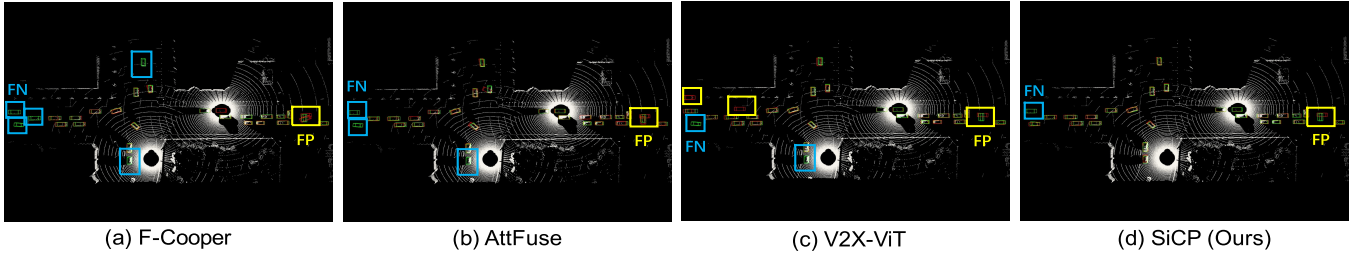


Figure 7. Illustrations of false positive (yellow) and false negative (blue) detection results for the cooperative perception scenarios.

Table 5. Impact of the 1x1 convolutional layer.

Method	Default		Culver	
	AP@0.5	AP@0.7	AP@0.5	AP@0.7
Mean	85.31	70.64	77.45	61.91
Max	85.16	71.54	77.87	61.89
Ours	85.72	73.64	77.49	62.42

Table 7. Impact of kernel sizes.

Kernel size	Default		Culver	
	AP@0.5	AP@0.7	AP@0.5	AP@0.7
1x1	84.67	70.74	77.45	61.73
3x3	85.72	73.64	77.49	62.42
5x5	85.82	73.35	76.71	62.05

to 2 results in a substantial improvement at both AP@0.5 and AP@0.7. This finding indicates that deeper feature extraction capabilities contribute to enhancing object detection performance. However, further increasing the number to 3 led to a marginal decline in performance, suggesting the presence of a saturation point specific to our task. Therefore, we select the default configuration of 2 layers with 3x3 convolutions to strike a balance between complexity and performance.

Table 6. Impact of different numbers of convolutional layers.

# of layers	Default		Culver	
	AP@0.5	AP@0.7	AP@0.5	AP@0.7
1	85.37	72.38	76.74	61.54
2	85.72	73.64	77.49	62.42
3	84.84	70.58	77.83	61.01

Impact of Kernel Size. Our results, as presented in Table 7, indicate that the 3x3 convolutional kernel consistently delivers the best overall performance. This finding indicates the popularity of the 3x3 kernel size in modern neural networks, attributed to its balanced combination of computational efficiency and feature-capturing capabilities.

5. Conclusions

In conclusion, this study shows how to realize simultaneous individual and cooperative perception for connected and automated vehicles. Our research demonstrates the feasibility of handling both tasks within a single model, leading to reduced memory usage in automated vehicles and minimized overall interference time. This solution is highly practical, given car manufacturers’ reluctance to implement separate models for individual and cooperative perception due to the associated high costs. The proposed DP-Net is versatile and can be seamlessly incorporated into other standalone 3D object detection models, empowering them with the capability of cooperative perception.

References

- [1] Eduardo Arnold, Mehrdad Dianati, Robert de Temple, and Saber Fallah. Cooperative perception for 3d object detection in driving scenarios using infrastructure sensors. *IEEE Transactions on Intelligent Transportation Systems*, 23(3): 1852–1864, 2020. 3
- [2] Qi Chen, Xu Ma, Sihai Tang, Jingda Guo, Qing Yang, and Song Fu. F-cooper: Feature based cooperative perception for autonomous vehicle edge computing system using 3d point

- clouds. In *2019 ACM/IEEE Symposium on Edge Computing (SEC)*, page 88–100. [1](#), [3](#), [6](#), [7](#)
- [3] Qi Chen, Sihai Tang, Qing Yang, and Song Fu. Cooper: Cooperative perception for connected autonomous vehicles based on 3d point clouds. In *2019 IEEE 39th International Conference on Distributed Computing Systems (ICDCS)*, pages 514–524. IEEE, 2019. [3](#)
- [4] Jiaxun Cui, Hang Qiu, Dian Chen, Peter Stone, and Yuke Zhu. Coopernaut: End-to-end driving with cooperative perception for networked vehicles. In *Proceedings of the IEEE/CVF Conference on Computer Vision and Pattern Recognition*, pages 17252–17262, 2022. [3](#)
- [5] Sudip Dhakal, Dominic Carrillo, Deyuan Qu, Qing Yang, and Song Fu. Sniffer faster r-cnn++: An efficient camera-lidar object detector with proposal refinement on fused candidates. *Journal on Autonomous Transportation Systems*, 2023. [3](#)
- [6] Sudip Dhakal, Qi Chen, Deyuan Qu, Dominic Carrillo, Qing Yang, and Song Fu. Sniffer faster r-cnn: A joint camera-lidar object detection framework with proposal refinement. In *2023 IEEE International Conference on Mobility, Operations, Services and Technologies (MOST)*, pages 1–10. IEEE, 2023. [3](#)
- [7] Alexey Dosovitskiy, German Ros, Felipe Codevilla, Antonio Lopez, and Vladlen Koltun. Carla: An open urban driving simulator. In *Conference on robot learning*, pages 1–16. PMLR, 2017. [6](#)
- [8] Chen Fu, Chiyu Dong, Christoph Mertz, and John M Dolan. Depth completion via inductive fusion of planar lidar and monocular camera. In *2020 IEEE/RSJ International Conference on Intelligent Robots and Systems (IROS)*, pages 10843–10848. IEEE, 2020. [3](#)
- [9] Jingda Guo, Dominic Carrillo, Sihai Tang, Qi Chen, Qing Yang, Song Fu, Xi Wang, Nannan Wang, and Paparao Palacharla. Coff: Cooperative spatial feature fusion for 3-d object detection on autonomous vehicles. *IEEE Internet of Things Journal*, 8(14):11078–11087, 2021. [3](#)
- [10] Yue Hu, Shaoheng Fang, Zixing Lei, Yiqi Zhong, and Siheng Chen. Where2comm: Communication-efficient collaborative perception via spatial confidence maps. *Advances in neural information processing systems*, 35:4874–4886, 2022. [1](#), [3](#), [6](#), [7](#)
- [11] Sergey Ioffe and Christian Szegedy. Batch normalization: Accelerating deep network training by reducing internal covariate shift. In *International conference on machine learning*, pages 448–456. pmlr, 2015. [5](#)
- [12] Diederik P Kingma and Jimmy Ba. Adam: A method for stochastic optimization. *arXiv preprint arXiv:1412.6980*, 2014. [6](#)
- [13] Alex H Lang, Sourabh Vora, Holger Caesar, Lubing Zhou, Jiong Yang, and Oscar Beijbom. Pointpillars: Fast encoders for object detection from point clouds. In *Proceedings of the IEEE/CVF conference on computer vision and pattern recognition*, pages 12697–12705, 2019. [1](#), [2](#), [3](#), [6](#), [7](#)
- [14] Yiming Li, Shunli Ren, Pengxiang Wu, Siheng Chen, Chen Feng, and Wenjun Zhang. Learning distilled collaboration graph for multi-agent perception. *Advances in Neural Information Processing Systems*, 34:29541–29552, 2021. [3](#)
- [15] Yifan Lu, Quanhao Li, Baoan Liu, Mehrdad Dianati, Chen Feng, Siheng Chen, and Yanfeng Wang. Robust collaborative 3d object detection in presence of pose errors. In *2023 IEEE International Conference on Robotics and Automation (ICRA)*, pages 4812–4818. IEEE, 2023. [2](#), [3](#), [4](#)
- [16] Chigozie Nwankpa, Winifred Ijomah, Anthony Gachagan, and Stephen Marshall. Activation functions: Comparison of trends in practice and research for deep learning. *arXiv preprint arXiv:1811.03378*, 2018. [5](#)
- [17] Charles R Qi, Hao Su, Kaichun Mo, and Leonidas J Guibas. Pointnet: Deep learning on point sets for 3d classification and segmentation. In *Proceedings of the IEEE conference on computer vision and pattern recognition*, pages 652–660, 2017. [3](#)
- [18] Charles Ruizhongtai Qi, Li Yi, Hao Su, and Leonidas J Guibas. Pointnet++: Deep hierarchical feature learning on point sets in a metric space. *Advances in neural information processing systems*, 30, 2017. [3](#)
- [19] Donghao Qiao and Farhana Zulkernine. Adaptive feature fusion for cooperative perception using lidar point clouds. In *Proceedings of the IEEE/CVF Winter Conference on Applications of Computer Vision*, pages 1186–1195, 2023. [3](#), [4](#)
- [20] Shaoshuai Shi, Xiaogang Wang, and Hongsheng Li. Pointcnn: 3d object proposal generation and detection from point cloud. In *Proceedings of the IEEE/CVF conference on computer vision and pattern recognition*, pages 770–779, 2019. [3](#)
- [21] Binglu Wang, Lei Zhang, Zhaozhong Wang, Yongqiang Zhao, and Tianfei Zhou. Core: Cooperative reconstruction for multi-agent perception. In *Proceedings of the IEEE/CVF International Conference on Computer Vision*, pages 8710–8720, 2023. [3](#), [4](#)
- [22] Tsun-Hsuan Wang, Sivabalan Manivasagam, Ming Liang, Bin Yang, Wenyuan Zeng, and Raquel Urtasun. V2vnet: Vehicle-to-vehicle communication for joint perception and prediction. In *European Conference on Computer Vision*, pages 605–621. Springer, 2020. [3](#)
- [23] Hao Xiang, Runsheng Xu, and Jiaqi Ma. Hm-vit: Heteromodal vehicle-to-vehicle cooperative perception with vision transformer. *arXiv preprint arXiv:2304.10628*, 2023. [3](#)
- [24] Runsheng Xu, Yi Guo, Xu Han, Xin Xia, Hao Xiang, and Jiaqi Ma. Opencda: an open cooperative driving automation framework integrated with co-simulation. In *2021 IEEE International Intelligent Transportation Systems Conference (ITSC)*, pages 1155–1162. IEEE, 2021. [6](#)
- [25] Runsheng Xu, Hao Xiang, Zhengzhong Tu, Xin Xia, Ming-Hsuan Yang, and Jiaqi Ma. V2x-vit: Vehicle-to-everything cooperative perception with vision transformer. In *European conference on computer vision*, pages 107–124. Springer, 2022. [1](#), [2](#), [3](#), [4](#), [6](#), [7](#)
- [26] Runsheng Xu, Hao Xiang, Xin Xia, Xu Han, Jinlong Li, and Jiaqi Ma. Opv2v: An open benchmark dataset and fusion pipeline for perception with vehicle-to-vehicle communication. In *2022 International Conference on Robotics and Automation (ICRA)*, pages 2583–2589. IEEE, 2022. [1](#), [2](#), [3](#), [4](#), [6](#), [7](#)

- [27] Yan Yan, Yuxing Mao, and Bo Li. Second: Sparsely embedded convolutional detection. *Sensors*, 18(10):3337, 2018. [3](#), [6](#), [7](#)
- [28] Bin Yang, Wenjie Luo, and Raquel Urtasun. Pixor: Real-time 3d object detection from point clouds. In *Proceedings of the IEEE conference on Computer Vision and Pattern Recognition*, pages 7652–7660, 2018. [6](#), [7](#)
- [29] Kun Yang, Dingkang Yang, Jingyu Zhang, Mingcheng Li, Yang Liu, Jing Liu, Hanqi Wang, Peng Sun, and Liang Song. Spatio-temporal domain awareness for multi-agent collaborative perception. In *Proceedings of the IEEE/CVF International Conference on Computer Vision*, pages 23383–23392, 2023. [3](#), [4](#)
- [30] Haibao Yu, Yizhen Luo, Mao Shu, Yiyi Huo, Zebang Yang, Yifeng Shi, Zhenglong Guo, Hanyu Li, Xing Hu, Jirui Yuan, et al. Dair-v2x: A large-scale dataset for vehicle-infrastructure cooperative 3d object detection. In *Proceedings of the IEEE/CVF Conference on Computer Vision and Pattern Recognition*, pages 21361–21370, 2022. [3](#)
- [31] Yin Zhou and Oncel Tuzel. Voxelnet: End-to-end learning for point cloud based 3d object detection. In *Proceedings of the IEEE conference on computer vision and pattern recognition*, pages 4490–4499, 2018. [3](#), [6](#), [7](#)